Modeling hysteresis and step response of a carbon-nanotube-reinforced electroactive actuator

Kiwon Sohn[1], Su Ryon Shin[1,2], Sun I. Kim[2], Byung-Ju Yi[3], Seon Jeong Kim[1,2]

[1]Center for Bio-Artificial Muscle,
Hanyang University, Seoul, South Korea
[2]Department of Biomedical Engineering,
Hanyang University, Seoul, South Korea
[3]School of Electrical Engineering and Computer Science,
Hanyang Unviersity, Ansan, South Korea

ABSTRACT

For polymer actuators, that are useful in wide variety of applications such as microelectromechanical systems (MEMS), machine components, and artificial muscles, the nonlinear phenomena of hysteresis and creep are essential considerations. We have investigated the movement of an electroactive polymer (EAP) actuator composed of single-wall carbon nanotubes (SWNTs) and polyaniline (PANI), and have developed an integrated model that can be used for simulating and predicting the hysteresis and creep during actuation.

We used the Preisach operator, one of the most popular phenomenological models of hysteresis, and the step response was depicted using the system identification technique. Understanding the behavior of the step response is especially important in open-loop control of the actuator.

In this paper, we present the mathematical description of our model as well as the extraction of the parameters. Simulation results from the model and a comparison with measured data are also provided.

Keywords: carbon nanotube, polyaniline, hysteresis, step response.

1 INTRODUCTION

Smart materials are called as polymer actuators and change their shape when electrical, chemical, thermal, or magnetic energy is applied to them. In particular, electroactive polymer (EAP) actuators that transform electrical energy into mechanical deformation have received much attention, because they are useful in a wide variety of nano/micro-sized applications, including microelectromechanical systems (MEMS),[1,2] drug delivery systems,[3] and nanomachine components.[4]

Polyaniline (PANI), which is an electroactive conducting polymer, functions via the reversible counter-ion insertion and expulsion that occurs during redox cycling, inducing a considerable change in volume that is mainly due to the exchange of ions with an electrolyte.[5] In a recent study, Spinks et al.[6] reported that the use of single-wall carbon nanotubes (SWNT) as reinforcing fibers in polyaniline improved the mechanical performance, and that an increase in breaking stress and a higher operating stress level were achieved.

For practical use of the PANI-SWNT composite as an EAP actuator, the kinetic characteristics, such as the hysteresis and step response, need to be identified.

Hysteretic behavior is observed in EAP actuators in such a way that applying the same electrical potential energy does not result in the same mechanical deformation. Ge et al.,[7] Lee et al.,[8] Croft et al.,[9] Song et al.,[10] Jung et al.,[11] and Changhai et al.[12] have studied hysteresis in piezoceramic actuators for precise positioning of materials, while Tan et al.[13] and Chen et al.[14] have modeled the hysteretic behavior of Ionic Polymer-Metal Composite (IPMC) actuators for similar reasons. Hysteresis models for shape memory alloy (SMA) actuators were also derived by Hasegawa et al.[15] and Choi et al.,[16] and a number of other researchers have employed various materials and theories to describe the hysteresis phenomena.[17–23]

Using system identification (SID) techniques, a step response of an EAP actuator was investigated by Yun et al.[24] for microscale PID control. This actuator was modeled employing an autoregressive moving average using an exogenous input (ARMAX) method and a chirp signal input from 0.01 to 1 Hz.

In this study, we investigated the hysteresis and step response of a PANI-SWNT composite EAP actuator modeled using the classical Preisach hysteresis model and an SID technique, respectively.

2 METHODS

2.1 Preparation of the PANI-SWNT composite EAP actuator

We prepared a PANI-SWNT composite EAP actuator employing the same method used in a previous study.[25] Acrylamido methylpropane sulfonic acid (AMPSA, 0.5 g) was dissolved in dichloroacetic acid (DCA, 20 mL), and SWNT (10 mg) was then added to the DCA–AMPSA solution. The resulting mixture was probe sonicated for a period of 1 h (in cycles of 2 s on and 1 s off) at room temperature using a Sonics and Materials Inc. (USA) 500W

Vibra cell. PANI emeraldine base (EB, 0.5 g) was slowly added to the SWNT dispersion, and the mixture was stirred under nitrogen at 2,000 rpm for 24 h, using a mechanical stirrer to obtain a green solution of the emeraldine salt (ES). The fiber was injected into a coagulation solution (acetone) bath through a 0.2 mm diameter syringe and a spinneret at a speed of 500 μl/min. The coagulation bath was rotated at 10 rpm, and the injected fiber was deposited at a distance of 2 cm from the rotation axis of the bath. The coagulated fibers were washed several times with deionized water and then suspended vertically in air and allowed to dry. The SWNT-based actuator sample was in the shape a ~1.5 cm-long fiber with a diameter of ~0.2 mm.

In the actuation experiments, we measured the variation in length of the SWNT-based EAP actuator while an electrical potential in the range 0.2–0.65 V was applied to the fiber.

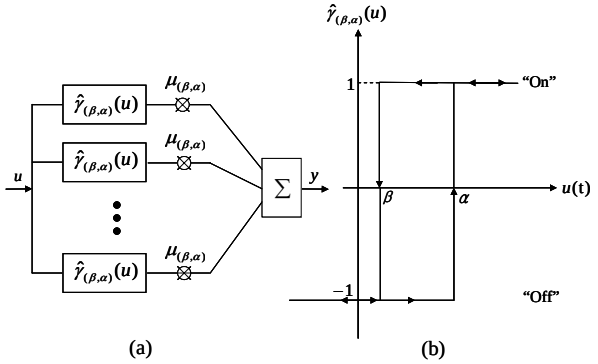

Figure 1. (a) The classical Preisach hysteresis model, and (b) the Preisach hysteron.

2.2 Preisach hysteresis model and identification of hysteresis in the actuator

The classical Preisach hysteresis model, which was first suggested to describe the hysteretic properties of ferromagnetism, is probably the most successful model of hysteresis. Since the Preisach model is a phenomenological model, any physical insight into the hysteresis is not implied. Therefore, it has been implemented in numerous applications and is now recognized as a fundamental tool in describing hysteretic phenomena.[26]

The Preisach hysteresis model is based on the principle of superposition. It exploits a parallel connection of pathways over Preisach hysterons $\hat{\gamma}_{(\beta,\alpha)}(u)$ and weight functions, $\mu_{(\beta,\alpha)}$, as shown Fig. 1 (a). An equation for the Preisach hysteresis model is

$$y(\mathrm{t}) = y_0 + \iint_{\alpha\geq\beta} \mu_{(\beta,\alpha)} \cdot \hat{\gamma}_{(\beta,\alpha)}[u(\mathrm{t})]d\alpha d\beta \qquad (1)$$

where $u(t) \in U_0 \equiv \{u \in \Re : u_{\min} \le u \le u_{\max}\}$, $(\beta,\alpha) \in P_0 \equiv \{(\beta,\alpha) \in \Re^2 : u_{\min} \le \beta \le \alpha \le u_{\max}\}$, and y_0 is the initial value of y(t), such that (β, α) = ($u_{\min}$, $u_{\min}$). Because each pathway in Fig. 1 (a) is assigned for each element of a set P_0, the output values for a given input, u, differ from one pathway to another. The Preisach hysteron in Fig. 1 (b) is equivalent to a simple nonlinear relay that is turned "on" or "off" by the two threshold numbers, α and β, respectively, where the outputs "on" and "off" correspond to 1 and –1, respectively. The threshold α is responsible for turning the hysteron on, while only β turns the Preisach hysteron off. In other words,

$$\hat{\gamma}_{(\beta,\alpha)}(u(\mathrm{t})) = \begin{cases} -1 & if \ \ (u(\mathrm{t}) < \beta) \\ & \vee \ \left[(\beta < u(\mathrm{t}) < \alpha) \ \wedge \ \left(\frac{du}{dt}(t) < 0 \right) \right] \\ 1 & if \ \ (u(\mathrm{t}) < \alpha) \\ & \vee \ \left[(\beta < u(\mathrm{t}) < \alpha) \ \wedge \ \left(\frac{du}{dt}(t) > 0 \right) \right]. \end{cases} \qquad (2)$$

Computing an output from a given input relies on an α-β diagram, which is a map of weight functions that characterizes the Preisach model. In the α-β diagrams in Fig. 2, the dots denote all pairs of (β, α) in a set, P_0, i.e., each dot denotes a weight function, $\mu_{(\beta,\alpha)}$, of the corresponding (β, α). In addition to an array of the weight functions, we defined a marker path, as shown in Fig. 2. Each dot in the marker path represents one of the elements in a set, U_0, and the marker has to be placed in the current input, u(t). The marker moves along the path as the input varies. Starting from the lowest end of the path, the marker jumps up to the next dot in the path as the input value increases. In contrast, the marker steps down when the input value decreases. Simple rules for the on-off status of the dots are as follows.

1. The marker is always "on".
2. When the input increases and the marker moves up one level, then all the dots in the same row that the marker is located in are turned "on".
3. When the input decreases and the marker moves down one level, then all the dots in the same column that the marker was previously located in are turned "off".

Figure 2 shows the on–off status of the dots when an input sequence [u_4 u_6 u_2 u_4] is applied. As shown in Fig. 2 (a), the first input is u_4, so that all the dots in rows u_1, u_2, u_3, and u_4 are "on". Figure 2 (b) shows the α-β diagram when the input increases to u_6. In Fig. 2 (c), as the marker moves down to u_2, all the dots in columns u_6, u_5, u_4, and u_3 are turned "off". Finally, Fig. 2 (d) shows the on–off status of the dots when the input increases to u_4 again. It should be noted that the left-hand two columns remain "on" at this time, which exemplifies why different outputs result from different extrema.

Repetitive step input procedures using the set of first-order transition curves identify the values of $\mu_{(\beta,\alpha)}$. In the identification process, the response from all the step inputs, whose number is the same as the number of weight functions, are measured in order. This results in the same

number of unknowns and equations and thus enables us to characterize the value of $\mu_{(\beta,\alpha)}$.

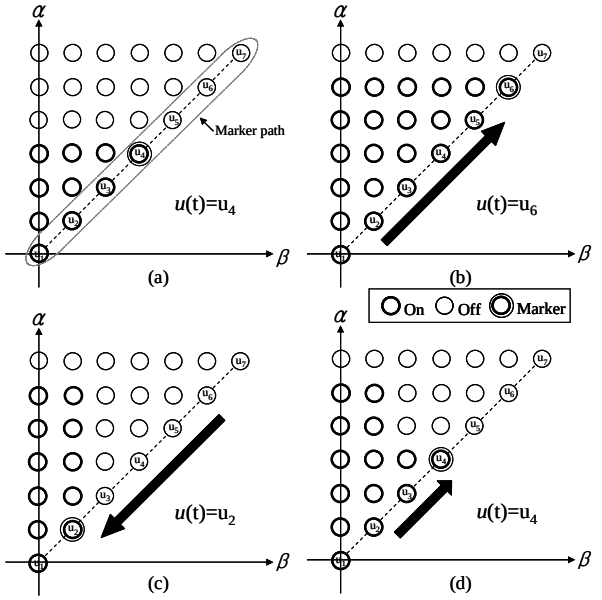

Figure 2. α-β diagrams that depict the on-off status of the weight functions. See the text for details.

Mathematically, $\mu_{(\beta,\alpha)}$ in the Preisach model is found by solving the following equation

$$\left[\sum_{(\beta,\alpha)=(u_{\min},u_{\min})}^{(u_{\max},u_{\max})} \mu_{(\beta,\alpha)} \cdot \hat{\gamma}_{(\beta,\alpha)}(u(\mathrm{k}))\right] = y(\mathrm{k}) - y_0 \qquad (3)$$

where u(k) is the k_{th} step input in the identification process and y(k) is a response during the k_{th} input. To obtain the correct response of a step input requires waiting until the response converges to a fixed value, and in our experiments, it took as long as 5 min for convergence to occur. A model of the hysteresis in the SWNT-based EAP actuator was established using our data.

2.3 System identification techniques and step response

An autoregression with exogenous input (ARX) method[27] was used to model the change in length to a step increase in the electrical input. The ARX method has the following standard form

$$A(\mathrm{q})y(\mathrm{t}) = B(\mathrm{q})u(\mathrm{t}) + e(\mathrm{t}), \qquad (4)$$

where A(q) and B(q) are parameters that derive from the input and output signals. The response of the actuator was measured after applying a step input of 0.4–0.45 V, which is the median range of possible inputs, 0.2–0.65 V. We assumed that the step response in the median range showed the same pattern as a step response shown throughout the range of 0.2–0.65 V.

3 SIMULATION RESULTS

3.1 Model of hysteresis

Using our model of the hysteresis, we simulated the hysteretic and inverse hysteretic behaviors to validate the model as well as to demonstrate our capability to predict the hysteresis.

In the validation of our model, we applied an arbitrary input sequence and compared the predicted outputs with the experimental results. Figure 3 (a) shows a simulated hysteresis loop and predicted output for a given applied input sequence. In Fig. 3 (b), the predicted outputs from the simulation overlap with the variation curve of the experimental outputs of the actuator.

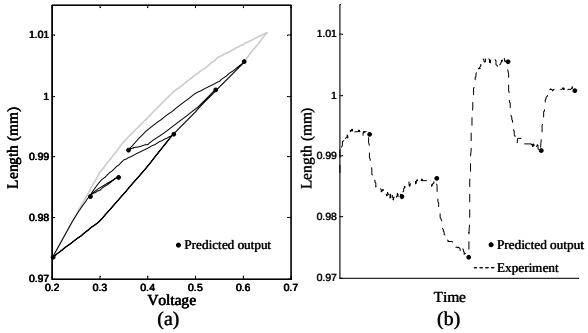

Figure 3. (a) Simulation of the hysteresis and outputs based on a given input sequence [0.45 V, 0.28 V, 0.34 V, 0.20 V, 0.60 V, 0.36 V, 0.54 V]. The gray line denotes the major hysteresis loop. (b) A comparison between the predicted outputs and the experimental data for a given input.

3.2 Model of the step response

Figures 4(a) and 4(b) show the output and input signals that were measured to identify the parameters of the ARX model, while Fig. 4 (c) shows a simulated step response using this model.

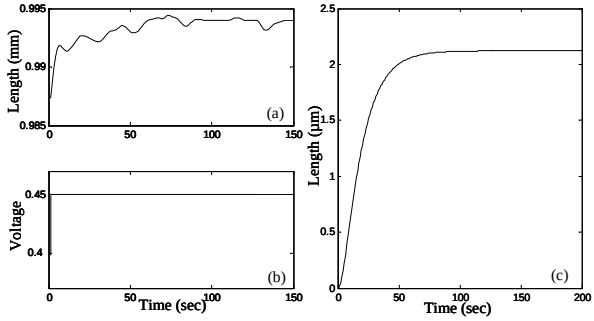

Figure 4. (a) The step response of the actuator. (b) The step input applied to the actuator. (c) Simulation of unit step response using the ARX method.

3.3 Simulation of the dynamics of PANI-SWNT composite EAP actuators

By combining the hysteresis and step response models,

we carried out simulations to predict the trajectory of the variation in length during the application of an input sequence, [0.45 V, 0.28 V, 0.34 V, 0.20 V, 0.60 V, 0.36 V, 0.54 V]. Figure 5 shows the simulated trajectory of the length overlaid on the data from Fig. 3. In the computation of the trajectory, the steady-state values denoted by the dots were predicted by our hysteresis model and then the transient curves between the dots, which were estimated using the ARX model.

Discrepancies appeared particularly for downward steps, and this may be because of the assumption that any single step response represented the step responses over the range of possible input values. Nonetheless, our simulation results showed the possibility of accurately predicting the dynamics of a PANI-SWNT composite EAP actuator during the application of an electrical input signal using a combined hysteresis and step response model.

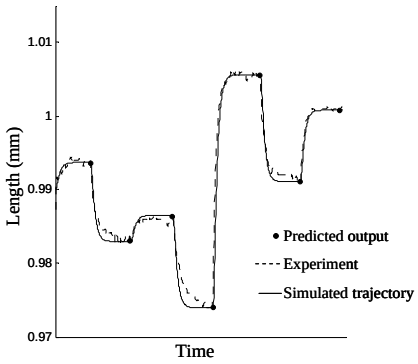

Figure 5. Simulation results from a combined hysteresis and a step response model superimposed on the data from Fig. 3 to show the trajectory of the variation in length. The input sequence is the same as used in Fig. 3.

4 CONCLUSIONS

PANI-SWNT composite EAP actuators and other conducting polymers have attracted much interest in various areas because they are convenient, safe, and power efficient. However, intensive research into the linear/nonlinear kinetic characteristics of EAP actuators has not been carried out. In this study, we have investigated the hysteresis and step response of an actuator using the classical Preisach hysteresis model and the SID technique, respectively, to demonstrate a predictive simulation for the trajectory of the variation in length, as the first step in continuing research that aims to show the precise and effective control of actuation.

ACKNOWLEDGEMENT

This work was supported by Creative Research Initiative Center for Bio-Artificial Muscle of the Ministry of Science & Technology (MOST) / the Korea Science and Engineering Foundation (KOSEF) in Korea.

REFERENCES

[1] Jager, E. W. H., Smela, E. and Inganas, O. (2000) *Science,* **290,** 1540–1545.
[2] Zhou, J. W. L., Chan, H. Y., To, T. K. H., Lai, K. W. C. and LI, W. J. (2004) *IEEE/ASME Trans. Mechatronics,* **9,** 334–342.
[3] Lobenberg, R. (2003) *Proceedings of the International Conference on MEMS, NANO and Smart Systems (ICMENS `03).*
[4] Collin, J. P., Dietrich-Buchecker, C., Gavina, P., Jimenez-Molero, M. and Sauvage, J. P. (2001) *Acc. Chem. Res.,* **34,** 477–487.
[5] Bar-Cohen, Y. (2001) *Electroactive polymer (EAP) actuators as artificial muscles,* SPIE Press, Bellingham, WA.
[6] Spinks, G. M., Mottaghitalab, V., Bahrami-Samani, M., Whitten, P. G. and Wallace, G. G. (2006) *Adv. Mater.,* **18,** 637–640.
[7] Ge, P. and Jouaneh, M. (1995) *Precis. Eng.,* **17,** 211–221.
[8] Lee, S.-H., Royston, T. J. and Friedman, G. (2000) *J. Intell. Mater. Syst. Struct.,* **11,** 781–790.
[9] Croft, D., Shed, G. and Devasia, S. (2001) *ASME J. Dyn. Syst. Meas. Control,* **123,** 35–43.
[10] Song, G., Zhao, J., Zhou, X. and DeAbreu-Garcia, A. (2005) *IEEE Trans. Mechatronics,* **10,** 198–208.
[11] Jung, H., Shim, J. Y. and Gweon, D. (2000) *Nanotechnology,* **12,** 14–20.
[12] Changhai, R. and Lining, S. (2005) *Sens. Actuators A,* **122,** 124–30.
[13] Tan, X., Baras, J. S. and Krishnaprasad, P. S. (2005) *Syst. Control Lett.,* **54,** 483–492.
[14] Chen, Z., Tan, X. and Shahinpoor, M. (2005) In *Proceedings of the IEEE/ASME International Conference on Advanced Intelligent Mechatronics,* Monterey, CA, pp. 60–65.
[15] Hasegawa, T. and Majima, S. (1998) In *International symposium on micromechatronics and human science* IEEE, pp. 171–176.
[16] Choi, B.-J., Lee, Y.-J. and Choi, B.-Y. (2004) *Smart Mater. Struct.,* **13,** 1069–1080.
[17] Spencer Jr., B. F., Dyke, S. J., Sain, M. K. and Carlson, J. D. (1997) *J. Eng. Mech.,* **123,** 230–238.
[18] Natale, C., Velardi, F. and Visone, C. (2001) *Physica B,* **306,** 161–165.
[19] Sakai, C., Ohmori, H. and Sano, A. (2003) In *Proceedings of the 42nd IEEE conference on decision and control,* pp. 3840–3845.
[20] Cavallo, A., Natale, C., Pirozzi, S. and Visone, C. (2003) *IEEE Trans. Magnetics,* **39,** 1389–1392.
[21] Dominguez, A., Sedaghati, R. and Stiharu, I. (2006) *Smart Mater. Struct.,* **15,** 1179–1189.
[22] Furuki, S., Terasawa, T. and Sano, A. (2006) In *Sice-ICASE International Joint Conference,* pp. 3228–3233.
[23] Wang, L. X. and Kamath, H. (2006) *Smart Mater. Struct.,* **15,** 1725–1733.
[24] Yun, K. and Kim, W.-J. (2006) *Smart Mater. Struct.,* **15,** 924–930.
[25] Sohn, K., Shin, S. R., Park, S. J., Yi, B.-J., Kim, S. I. and Kim, S. J. (2007) *J. Nanosci. Nanotechnol.,* **Submitted**.
[26] Mayergoyz, I. D. (2003) *Mathematical models of hysteresis and their applications,* Elsevier.
[27] Ljung, L. (1999) *System Identification: Theory for the Users, 2nd edition,* Prentice Hall, Upper Saddle River, NJ.